Neuropeptide Release Is Impaired in a Mouse Model of Fragile X Mental Retardation Syndrome

Suresh P. Annangudi,[†,⊥] Agatha E. Luszpak,[†,‡,§] Soong Ho Kim,[†,‡] Shifang Ren,[†,⊥] Nathan G. Hatcher,[†,⊥] Ivan Jeanne Weiler,[†,‡] Keith T. Thornley,[▽] Brian M. Kile,[▽] R. Mark Wightman,[▽] William T. Greenough,*[,†,‡,∥] and Jonathan V. Sweedler*[,†,‡,⊥]

[†]Beckman Institute, [‡]Neuroscience Program, [§]Medical Scholars Program, [⊥]Department of Chemistry, and [∥]Departments of Psychology, Psychiatry, and Cell and Structural Biology, University of Illinois at Urbana−Champaign, Urbana, Illinois 61801, and [▽]Department of Chemistry, University of North Carolina at Chapel Hill, Chapel Hill, North Carolina 27514

Abstract

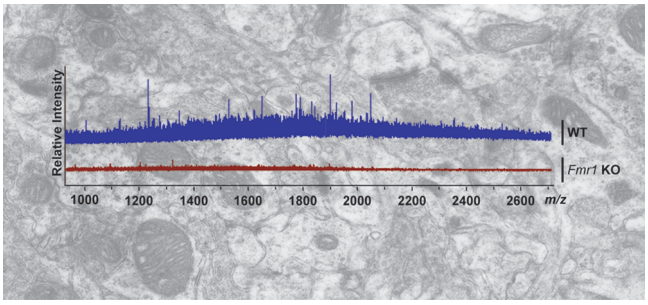

Fragile X syndrome (FXS), an inherited disorder characterized by mental retardation and autism-like behaviors, is caused by the failure to transcribe the gene for fragile X mental retardation protein (FMRP), a translational regulator and transporter of select mRNAs. FXS model mice (*Fmr1* KO mice) exhibit impaired neuropeptide release. Release of biogenic amines does not differ between wild-type (WT) and *Fmr1* KO mice. Rab3A, an mRNA cargo of FMRP involved in the recruitment of vesicles, is decreased by ∼50% in synaptoneurosomes of *Fmr1* KO mice; however, the number of dense-core vesicles (DCVs) does not differ between WT and *Fmr1* KO mice. Therefore, deficits associated with FXS may reflect this aberrant vesicle release, specifically involving docking and fusion of peptidergic DCVs, and may lead to defective maturation and maintenance of synaptic connections.

Keywords: Neuropeptide release, Rab3A, dense-core vesicles, Fragile X syndrome, synaptic remodeling, dendrites, mass spectrometry, synaptic transmission

Fragile X syndrome (FXS) is the most common cause of inherited mental retardation, with an incidence of 1 in 4000 males and 1 in 8000 females (*1*). The molecular mechanism underlying FXS involves the expansion of an unstable polymorphic CGG triplet repeat to >200 in the 5′ untranslated region of the *Fmr1* gene (*2*, *3*). This results in hypermethylation of the *Fmr1* promoter and silencing of the *Fmr1* gene, with consequent absence of the protein product, fragile X mental retardation protein (FMRP) (*3*). FMRP is an mRNA-binding protein that is enriched at the synapse and known to regulate the transport and localized translation of mRNA in response to mGluR receptor activation (*4*). Many of the mRNA cargoes associated with FMRP encode proteins crucial for spine maturation and synaptic plasticity (*5*−*8*).

In the absence of FMRP, there is defective regulation of localized mRNA translation. This absence affects synaptic plasticity in FXS, with abnormalities in long-term potentiation (LTP) and long-term depression (LTD) (*9*, *10*) in *Fmr1* knockout (KO) mice, which exhibit characteristics of FXS (*11*, *12*). The absence of FMRP should lead to dysregulated local protein levels in both axons and dendrites, but previous reports have focused largely on translational regulation deficits at the postsynaptic site in FXS. Studies by Hanson and Madison (*13*) and Lauterborn et al. (*14*) recently suggested possible presynaptic effects caused by the loss of FMRP, prompting us to examine neuropeptide release in FXS. The mRNA cargoes of FMRP include presynaptic proteins that participate in the secretory pathway, in particular, vesicle exocytosis (*5*, *6*). One such protein is Rab3A, a GTPase that cycles between a soluble Rab3A-GDP form and a vesicle membrane-bound Rab3A-GTP form and is involved in activity-dependent vesicle docking and fusion at the synapse (*15*, *16*). Changes in Rab3A levels would be expected to affect activity-dependent release of transmitters and modulators. Using Western blot analyses, we characterized the levels of this protein in wild-type (WT) and *Fmr1* KO mice.

Next, we used matrix-assisted laser desorption/ionization (MALDI) mass spectrometry (MS) to examine

Received Date: November 24, 2009
Accepted Date: December 17, 2009
Published on Web Date: January 08, 2010

© 2010 American Chemical Society

DOI: 10.1021/cn900036x | *ACS Chem. Neurosci.* (2010), *1*, 306–314

synaptoneurosomal preparations and probed the physiology of stimulus-evoked neuropeptide release in *Fmr1* KO mice using live brain slices. Our results indicate that these mice are markedly deficient in neuropeptide release. In order to determine whether the neuropeptide release deficit in *Fmr1* KO mice is a general deficit in dense-core vesicle (DCV) release, we used electrochemistry to examine the release of biogenic amines. We show that the release deficit is specific to peptides, because there is no significant difference in the release of dopamine (DA), serotonin (5-HT), and norepinephrine (NE) from the striatum of WT and *Fmr1* KO mice. Lastly, using electron microscopy to quantify the number of peptide-housing DCVs, we do not observe significant differences between WT and *Fmr1* KO mice, again suggesting a specific release deficit in FXS.

Results and Discussion

Levels of Rab3A in WT and *Fmr1* KO Mouse Brains

We characterized the amount of Rab3A at the synapse using synaptoneurosomal preparations, which are enriched in intact pinched-off synaptic processes, from postnatal 10−14 day (P10−14) WT and *Fmr1* KO mice. Using Western blot analysis, we found Rab3A expression to be reduced by ∼50% in isolated cortical synapses of *Fmr1* KO mice ($n = 8$) compared with that in WT mice ($n = 8$; $p < 0.01$) (Figure 1a,b). The amount of Rab3A in total cortical homogenates was also decreased in the *Fmr1* KO mice, however, to a smaller extent, because total homogenates contain more somatic material (Figure 1c, $n = 4$, WT; $n = 4$, *Fmr1* KO; $p < 0.01$).

The decrease in Rab3A may be accompanied by a decrease in Rab3 interacting proteins. Liao et al. (*17*) recently reported reduced protein levels of other Rab isoforms in *Fmr1* KO mice, including several proteins involved in vesicle exocytosis. Rab3A KO mice have previously been shown to have altered activity-dependent vesicle release (*15*) and complete loss of LTP at the hippocampal CA3 mossy fiber synapses (*18*). Although the mechanism behind Rab3A function in FXS is currently unknown, we speculate that there may be an imbalance in Rab3A-GDP and Rab3A-GTP cycling. It has previously been shown that an accumulation of membrane-bound Rab3A-GTP leads to a reduction in docked DCVs (*19*). Van Weering et al. (*20*) have observed that neither Rab3A-GTP- nor Rab3A-GDP-locked mutant chromaffin cells exhibited any differences in the total amount of DCVs as compared with WT chromaffin cells.

Neuropeptide Release

To directly investigate whether there is a peptide release deficit associated with reduced Rab3A, we developed a MS-based protocol to examine stimulation-dependent release of peptides from WT and *Fmr1* KO mouse cortical synaptoneurosomes. Previously reported methods primarily used electrophysiology to observe the effects of stimulation at *Fmr1* KO mouse synapses (*21*). Synaptosomes have been used for many studies on neurotransmitter release (*22*). Here, we adapted small-volume (*23*, *24*) and neuropeptide release collection approaches (*25*−*28*) to enable MS-based peptide characterization of released peptides in *Fmr1* KO mice. Briefly, synaptoneurosomal preparations from WT and *Fmr1* KO mice ($n = 4$, WT; $n = 5$, *Fmr1* KO) were stimulated with KCl (55 mM), and the releasates were concentrated and separated into fractions using reversed-phase liquid chromatography (LC). The fractions were analyzed using MALDI-MS. The resulting mass profiles of releasates from WT cortical synaptoneurosomes revealed stimulation-dependent release of several peptide signaling molecules as well as protein fragments (Figure 2a). Little or no stimulated peptide release was observed in cortical synaptoneurosomes from *Fmr1* KO mice; the reduction in peptide release is at least 90% and perhaps greater (Figure 2c), with the large decrease making quantitative measures of decrease difficult. To consider whether the KCl stimulation data reflect presynaptic or postsynaptic peptide release events, (*S*)-3,5-dihydroxyphenylglycine (DHPG) was administered to stimulate postsynaptic group I metabotropic glutamate receptors in the WT

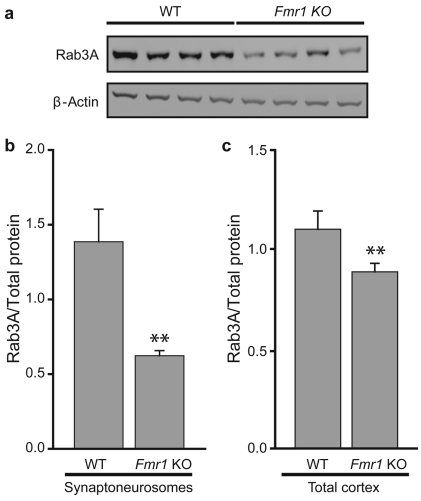

Figure 1. Western blot analysis from P10−14 WT and *Fmr1* KO mouse cortical synaptoneurosomes and total cortical homogenates shows a reduction in Rab3A expression. (a) Synaptoneurosomal lysates from WT and *Fmr1* KO mouse cortices were run on 12% polyacrylamide gels, blotted to nitrocellulose membranes, and stained with rabbit polyclonal antibody specific for Rab3A, followed by antibody to β-actin to normalize to total protein loaded. (b) Rab3A expression in *Fmr1* KO mouse synaptoneurosomes ($n = 8$) is dramatically reduced compared with that in WT mouse synaptoneurosomes ($n = 8$). Blots were normalized to β-actin (β-actin, **, $p < 0.01$; not shown) and to total protein loaded (**, $p < 0.01$; error bars, SEM). (c) Rab3A expression in total cortical homogenates is significantly decreased in *Fmr1* KO mice, although to a smaller extent than in synaptoneurosomes ($n = 4$; **, $p < 0.01$).

© 2010 American Chemical Society

DOI: 10.1021/cn900036x | *ACS Chem. Neurosci.* (2010), *1*, 306–314

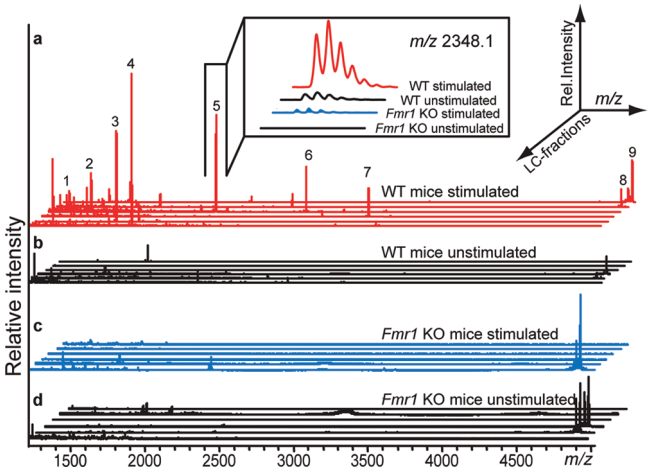

Figure 2. Synaptoneurosomes from *Fmr1* KO mice are defective in neuropeptide release. LC−MALDI-MS analysis of releasates collected from stimulated (KCl, 55 mM) and unstimulated (saline) cortical synaptoneurosomes from P10−14 WT and *Fmr1* KO mice. Each panel represents a profile in the mass range m/z 1300−5000 of several LC fractions for (a, b) WT and (c, d) *Fmr1* KO mice. The mass profiles obtained from the releasates of stimulated WT synaptoneurosomes (a) show a number of high-intensity peaks compared with those from the *Fmr1* KO synaptoneurosomes (b). Using MS/MS analysis or accurate mass match, we identified several peaks as peptides derived from (1) PEP-19, (2) cholecystokinin 12, (3) unknown m/z 1776.7, (4) unknown m/z 1923.7, (5) stathmin (6) orexin B, (7) unknown m/z 3387.0, (8) thymosin β4, and (9) thymosin β10. Inset shows an expanded mass region from the fraction containing stathmin peptide at m/z 2348.1.

synaptoneurosomes; this stimulation did not elicit synaptic peptide release. Thus, we suggest, but have not yet fully confirmed, that this deficit is presynaptic in nature. Several peptides and protein fragments observed in the releasates of stimulated WT synaptoneurosomes were present in sufficient amounts to confirm their identity with tandem MS (MS/MS) analysis. These peptides are primarily derived from structural and related proteins (such as actin, tubulin, and stathmin) and neuropeptide prohormones (Supporting Information, Table S1).

To confirm changes in the stimulation-induced release in a more intact preparation, we used brain slices obtained from P10−15 WT and *Fmr1* KO mice, as described earlier (*25*). We chose two regions to study: (1) the cerebral cortex, because this was the source of our synaptoneurosomes, and (2) the suprachiasmatic nucleus (SCN), a well-defined nucleus that is highly peptidergic and for which we previously characterized robust peptide release (*25*). Using an on-tissue collection strategy, we collected releasates from the cortex and SCN of WT and *Fmr1* KO mice using a micropipet tip packed with C18 solid-phase extraction beads. We then performed MALDI-MS analysis on releasates obtained before and after stimulation with 55 mM KCl. The MS profiles showed a significant increase in the number and intensity of peaks detected in releasates after stimulation of WT, but not KO slices, compared with the prestimulated collections (Figure 3, n = 4, WT; n = 4, *Fmr1* KO). In addition to arginine vasopressin, somatostatin, and proSAAS, which have been shown earlier to be released from the SCN (*25*), we identified several peptides from the cortex that were also identified from the synaptoneurosomal releasates.

Although we have shown that the impaired release mechanisms involve peptides, it is reasonable to speculate that other regulated release pathways might be affected, such as cytokine and growth factor release. For example, brain-derived neurotrophic factor (BDNF) release from CA3 neurons was shown to recruit a presynaptic component of plasticity (*29*). Lauterborn et al. (*14*) recently showed that the LTP deficiency observed in the hippocampal field CA1 of *Fmr1* KO mice can be rescued by exogenous application of BDNF, even though there was no significant difference in the basal level of BDNF in homogenates of *Fmr1* KO versus WT hippocampus; therefore, those results also imply a deficit in BDNF synaptic release in FXS.

Biogenic Amine Release in Brain Slices

To analyze the specificity of the observed release deficit, we used electrochemistry-based measurements to analyze the stimulus-evoked release of biogenic amines. Brain slices from P70 WT and *Fmr1* KO mice containing the caudate putamen (CP), ventral bed nucleus of the stria terminalis (vBNST), or substantia nigra pars reticulata (SNr) were used to analyze the electrically stimulated release of DA, NE, and 5-HT, respectively, because these particular regions are enriched in these biogenic amines (*30*−*32*). DA release in striatal brain slices was evoked by a single-pulse electrical stimulation (Figure 4a). Stimulated release of 5-HT (20 pulses at 20 Hz) in slices of the SNr had a similar profile; however, the maximal release values and rate of uptake are both lower than those seen for DA (Figure 4b). NE release was evoked by 60 pulses at 60 Hz stimulation and demonstrated the slowest uptake of all three neurotransmitters (Figure 4c). Electrically stimulated DA release monitored by fast-scan cyclic voltammetry was unchanged in *Fmr1* KO mice compared with WT mice (n = 6, WT; n = 7, *Fmr1* KO; $p > 0.05$). Additionally, NE release in the vBNST stimulation was not different (n = 4, WT; n = 6, *Fmr1* KO; $p > 0.05$) between *Fmr1* KO and WT control animals. This trend was repeated in the SNr where stimulation evoked the same amount of 5-HT in both animals (n = 6, WT; n = 7, *Fmr1* KO; $p > 0.05$). Similar results were found when monitoring exocytosis from chromaffin cells (Supporting Information, Figure S1 and Table S2). The lack of differences in release of biogenic amines between WT and *Fmr1* KO mice shows that the presynaptic release deficit is not general but is transmitter specific.

© 2010 American Chemical Society

DOI: 10.1021/cn900036x | *ACS Chem. Neurosci.* (2010), *1*, 306–314

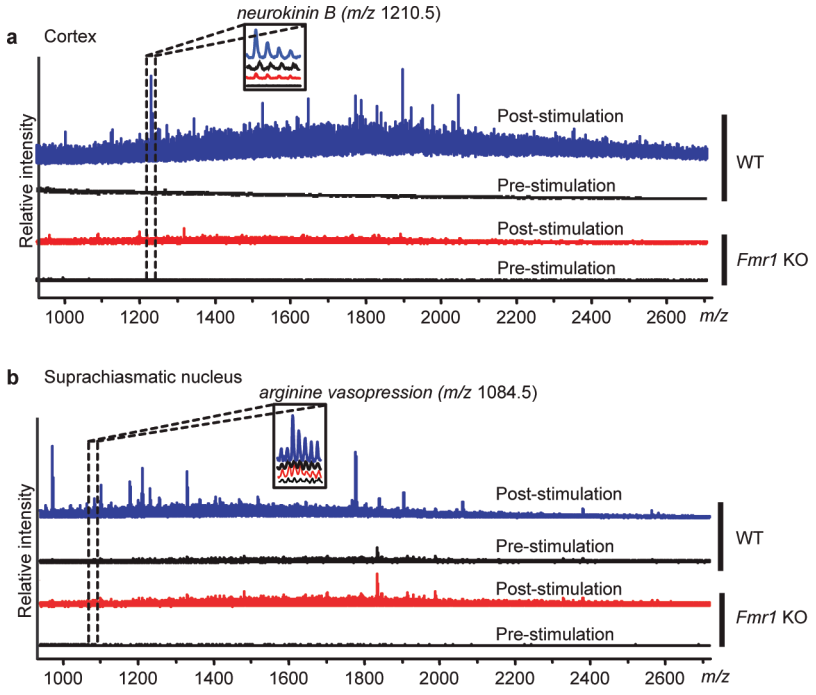

Figure 3. Defective neuropeptide release from *Fmr1* KO brain slice preparations. MALDI-MS analysis of releasates from whole brain slices (400 μm) containing SCN and cortex from P10−15 WT and *Fmr1* KO mice. Slices stimulated with a topical application of 55 mM KCl show marked increase in the number and intensity of peptides observed in WT mice compared with *Fmr1* KO mice ($n = 4$, WT; $n = 4$, *Fmr1* KO). (a) Mass profiles obtained from the cortex and (b) from the SCN. Inset in panel a shows relative intensity of neurokinin B and inset in panel b shows arginine vasopressin, for all four conditions.

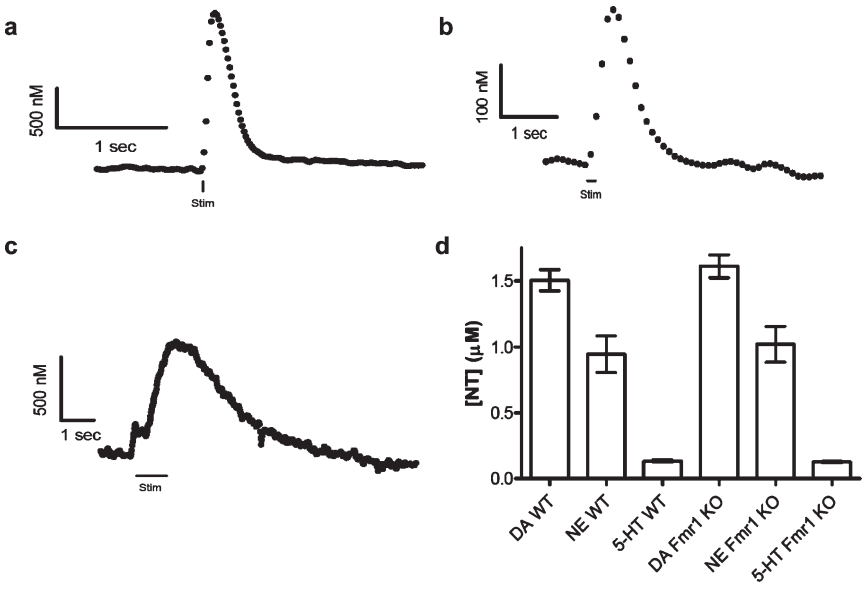

Figure 4. Biogenic amine (DA, NE, 5-HT) release from WT and *Fmr1* KO brain slice preparations is not significantly different: (a) DA release in the CP evoked with a single stimulus pulse; (b) 5-HT release evoked in the SNr by a 20 pulse, 100 Hz stimulation train; (c) NE release in the BNST evoked by a 60 pulse, 60 Hz stimulation (data shown are from WT tissues); (d) identical release concentrations were observed in brain slices from WT and *Fmr1* KO ($p > 0.05$, $n = 6$ from each genotype for each neurotransmitter).

Quantification of Dense-Core Vesicles

It is known that both clear-core vesicles, which house many classical neurotransmitters, and large DCVs, which house peptides and perhaps the catecholamines, are mobilized and released in an activity-dependent manner (*33*, *34*). Because DCVs contain neuropeptides, we considered whether the decrease in the amount of peptides observed in *Fmr1* KO mice was due to

© 2010 American Chemical Society

DOI: 10.1021/cn900036x | *ACS Chem. Neurosci.* (2010), *1*, 306–314

a decrease in the number of DCVs. We examined electron micrographs containing layer IV of the visual cortex from P15 and P25 WT and *Fmr1* KO mice, utilizing unbiased stereological methods to look for differences in the density of DCVs (DCVs/μm^3). While a decrease in DCVs/μm^3 between WT and *Fmr1* KO mice at both P15 and P25 was observed (Supporting Information, Figure S2), these differences did not reach significance. A significant decrease in DCVs/μm^3 from P15 to P25 was observed for both genotypes. Specifically, our analysis revealed a main effect of age ($p < 0.01$) but no main effect of genotype ($p = 0.220$) and no genotype−age interaction ($p = 0.996$).

Conclusions

MS-based assays that are capable of analyzing release enable characterization of peptide secretion following chemical stimulation, without having to preselect the peptides (*25*, *26*, *35*). The ability to collect and characterize peptide release allows us to present the first report of impaired peptidergic release in the FXS mouse model. Although there is not a significant reduction of DCVs in FXS, there is a ∼50% reduction in synaptic levels of Rab3A. These results suggest that some of the deficits in *Fmr1* KO mice may be directly correlated with deficits in the peptide release machinery. Intriguingly, the release deficit observed in the *Fmr1* KO mice involves the release of neuropeptides in the neocortex and does not involve biogenic amines in the striatum, suggesting a deficit in the release of peptidergic DCVs, at least in several brain regions of FXS mice. Because similar reductions in peptide release are observed in both functional synapses (synaptoneurosomes) and brain slices from the cerebral cortex and the SCN, this impairment appears to be fairly general and may be associated with synaptic machinery, perhaps aberrant DCV docking and fusion, in which Rab3A normally participates. Stimulated release of DA, NE, and 5-HT is unaffected in the striatum, and basal synaptic transmission in *Fmr1* KO mice is similar to WT mice (*36*), results that point to a specific release defect in the brain.

In conclusion, there appears to be a role for cell-to-cell signaling in the etiology of FXS, possibly affecting one or more phases of the synaptogenesis and synaptic stabilization sequence (*37*, *38*). Peptides characterized as released from the synapses in an activity-dependent manner include fragments of structural proteins such as actin, tubulin, and stathmin, which are involved in exocytosis. Their dynamics play a role in the morphological plasticity of dendritic spines (*39*), and release of these peptides is reduced in *Fmr1* KO mice. The resilience of this defect, as observed in synaptoneurosomes and slice preparations from several brain regions, suggests that this impaired peptide-specific release may be a fundamental biological deficit and may contribute to defective synaptic maturation and maintenance and the behavioral deficits known to be associated with FXS. The correlation between FXS and the neuropeptide release deficit suggests that this is a unique pharmacological target, which, if restored, may ameliorate some of the effects of FXS.

Methods

Animals

WT and sighted *Fmr1* KO mice bred in the FVB.129P2-*Fmr1*^{tm1Cgr} background were housed at the Beckman Institute at the University of Illinois at Urbana−Champaign (UIUC) or the University of North Carolina at Chapel Hill (UNC−CH) animal facility. Mice were maintained under controlled environmental conditions, with standard alternating periods of 12-h light and darkness. Rodent chow and water were provided *ad libitum*. Animal care and procedures in accordance with the National Institutes of Health regulations and protocols were approved by the UIUC and UNC−CH Institutional Animal Care and Use Committees.

Synaptoneurosomal and Total Cortical Homogenate Preparation

Synaptoneurosomes were prepared from cortices of P10−14 WT and *Fmr1* KO mice. For the MS measurements of synaptoneurosome release only, six experiments were performed using rat cortices to validate our ability to stimulate peptides and collect releasates ($n = 6$). Once the ability to collect peptide release was shown to be robust, we modified the procedures for smaller mouse samples. Briefly, mice were sacrificed by decapitation. Brains were removed and dissected, and several cerebral cortices were pooled to obtain adequate cellular material for each experiment ($n = 4$, WT; $n = 5$, *Fmr1* KO with each sample consisting of two or three cortices). Cortices were homogenized in a glass−Teflon homogenizer in 1 mL of ice-cold homogenizing buffer (50 mM *N*-2-hydroxyethylpiperazine-*N*′-2-ethanesulfonic acid (HEPES), pH 7.5, 125 mM NaCl, 100 mM sucrose, 2 mM potassium acetate), filtered through a series of nylon mesh filters (149, 62, 30, and 10 μm; Small Parts, Inc., Miramar, FL) and finally filtered through a 10-μm polypropylene filter (Gelman Sciences, Ann Arbor, MI). Filters were washed at each step with the ice-cold homogenizing buffer. The final filtrate was spun briefly (4000 × *g*, 4 °C, 1 min) to remove cellular debris; final supernatant volume was ∼1 mL. This synaptoneurosomal preparation was either used directly for stimulation and collection of releasates by MS or was lysed (for Western blot analysis) in a lysis buffer [final concentration 50 mM Tris (pH 8), 150 mM NaCl, 1% Nonidet P-40, 20 nM okadaic acid, 20 μM sodium orthovanadate, phosphatase inhibitor mixture (Pierce, Rockford, IL), and protease inhibitor mixture (Roche, Indianapolis, IN)]. NP-40 soluble total cortical homogenate was prepared in the following way: cortices from a single mouse, P10−14, were homogenized in NP-40 lysis buffer [final concentration 50 mM Tris (pH 8), 150 mM NaCl, 1% Nonidet P-40, 20 nM okadaic acid, 20 μM sodium orthovanadate, phosphatase inhibitor mixture (Pierce), and

© 2010 American Chemical Society

DOI: 10.1021/cn900036x | *ACS Chem. Neurosci.* (2010), *1*, 306–314

protease inhibitor mixture (Roche)] and spun (15 000 × *g*, 4 °C, 15 min), and then the supernatant was collected.

Western Blot Analysis

For each synaptoneurosomal preparation and total cortical homogenate sample, 30 μg of lysed protein samples was run on 12% polyacrylamide gels, blotted to nitrocellulose membranes, and stained with rabbit polyclonal antibody specific for Rab3A (Abcam, Cambridge, MA). HRP-labeled secondary antirabbit antibody (Cell Signaling Technology, Inc., Danvers, MA) was detected by enhanced chemiluminescence (Pierce). To quantify and standardize protein levels, blots were stained for β-actin (Sigma Aldrich, St. Louis, MO) and with Amido Black (J. T. Baker, Phillipsburg, NJ) for total protein. Chemiluminescence was scanned in a FluorChem 8900 Imager (Alpha Innotech, San Leandro, CA) and relative optical densities were determined by using AlphaEaseFC software, version 4.0.1 (Alpha Innotech), normalized to β-actin level and total protein loaded.

Synaptoneurosomal Stimulation

The synaptoneurosomal preparations, obtained from two to three mouse cerebral cortices for each preparation, were divided into two equal aliquots used as a control (unstimulated) or as the stimulated sample. For the stimulated samples, 1 M KCl (55 mM final concentration) or 1 M DHPG (Tocris Cookson, Ellisville, MO; 5 mM final concentration), was added to one of the aliquots and incubated for 15 min. For the control samples, 50 μL of homogenizing buffer was added. After stimulation, the aliquots were centrifuged (4 min at 4000 × *g* at 4 °C), and the supernatant was collected. The peptides present in the supernatant were desalted and concentrated using a spin-column (Pierce) according to the manufacturer's protocols. These measurements were repeated for nine samples (from 21 animals). In two instances, after chemical stimulation, no peptides (including the normally ubiquitous β-thymosin) were detected via MS, indicating an issue with the preparation; in such cases, the data were excluded.

Brain Slice Preparation and Stimulation

Brain slices were prepared from P10−P15 WT and *Fmr1* KO mice. Briefly, mice were quickly decapitated, brains were removed, and a Vibratome (Vibratome 3000 Series; Ted Pella, Redding, CA) was used to obtain 400-μm sections. The sections were placed into a brain slice chamber (AutoMate Scientific, Inc., Berkeley, CA) equipped with a proportional temperature controller. Each slice was perfused with Earle's balanced salt solution (EBSS; without phenol red), supplemented with 24.6 mM glucose, 26.2 mM $NaHCO_3$, and 2.5 mg/L gentamycin and saturated with 95% O_2/5% CO_2 at 37 °C, pH 7.4. Collection of releasates from each slice (n = 4, WT; n = 4, *Fmr1* KO) was performed as described earlier (*25*) and analyzed by MALDI-MS.

Liquid Chromatography

The synaptoneurosomal releasates were separated using a capLC system (Micromass, U.K.) coupled to a robotic spotter (Proteineerfc, Bruker Daltonics, Billerica, MA). Briefly, the samples were initially loaded onto a 5-μL loop using a manual injector (VALCO Instruments Co. Inc., Houston, TX) and subsequently trapped onto a reversed-phase trap column (PepMap, C18, 5 μm, 100 Å, LC Packings, a Dionex Company, Sunnyvale, CA) using solvent C (90% water, 10% acetonitrile (ACN), 0.1% formic acid (FA), and 0.01% trifluoroacetic acid (TFA)) at a flow rate of 8 μL/min and washed for 5 min. Each sample was then eluted and separated on a reversed-phase column (LC Packings 300-μm i.d. × 15 cm, C18 PepMap100, 100 Å) using a gradient at 2 μL/min flow rate for 45 min. Gradients were generated using solvent A (95% water, 5% ACN, 0.1% TFA) and solvent B (95% ACN, 5% water, 0.1% FA, and 0.01% TFA). Gradients were changed linearly in three different steps; 5−30% solvent B in 15 min, 30−80% solvent B in 35 min, 80−5% solvent B in 40 min. The chromatographic profile was monitored using a UV detector at 210 nm. The capLC system was connected online to the Proteineerfc spotter to collect the fractions onto a MALDI target. Prior to spotting the fractions, the Proteineerfc was programmed to deposit 1 μL of α-cyano-4-hydroxy cinnamic acid MALDI matrix (10 mg/mL, 60% aqueous ACN, 0.1% TFA). For each sample, a total of 24 fractions were collected at 1 min intervals, corresponding to samples eluted from 18−42 min of the chromatographic run.

Mass Spectrometry

Mass spectrometric analysis of the samples was performed using a MALDI-TOF/TOF mass spectrometer (Ultraflex II, Bruker Daltonics). The instrument was externally calibrated using a mixture of standard peptides (angiotensin II, angiotensin I, substance P, bombesin, ACTH clip 1−17, ACTH clip 18−39, somatostatin 28, bradykinin fragment 1−7, renin substrate tetradecapeptide porcine) in the mass range 700−3200 Da (Bruker Daltonics). For each of the synaptoneurosomal releasate fractions, data was collected using 400 laser shots in 10 short steps by panning across the spot and combining the spectra. Following data collection, the mass spectra were smoothed and baseline corrected, and the peaks with high peak intensity and signal/noise ratio were tabulated. Releasates from the slice were directly analyzed using MALDI-MS.

MS/MS of selected molecular ion species was performed using the TOF/TOF feature of the Bruker Ultraflex II instrument. The MS/MS spectra were processed using FlexAnalysis 2.4 and Biotools 3.0 software packages (Bruker Daltonics). Partial *de novo* analysis was also performed on the MS/MS spectra using Peaks software (Bioinformatics Solutions Inc., Waterloo, Ontario, Canada) to assist in peptide identification. For the release of peptides from the SCN, previously sequenced peptides characterized in the SCN and supraoptic nucleus were used for peptide identification (*25*, *40*).

Electron Microscopy and DCV Quantification

Eight P15 WT and ten P15 *Fmr1* KO mice and eight P25 WT and ten P25 *Fmr1* KO mice were used to analyze DCV quantity in layer IV of the visual cortex. Perfusion and tissue preparation procedures for transmission electron microscopy ultrastructural analyses of brain have been described in a previous report (*41*). Within layer IV of the visual cortex, a region of neuropil was selected based *only* on proximity to easily recognizable landmarks (capillaries, nuclei, etc.) and on the absence of folds in adjacent sections (aside from these two criteria, the region was selected randomly within layer IV). Micrographs from identical regions of consecutive (approximately 60-nm thick) serial sections were

© 2010 American Chemical Society

DOI: 10.1021/cn900036x | *ACS Chem. Neurosci.* (2010), *1*, 306–314

taken at a magnification of 8800× (final magnification 26,400×) by a Phillips CM-200 transmission electron microscope and analyzed by raters blind to the experimental group. The density of DCVs was estimated using the physical disector (*42*), in which disector pairs, composed of a "reference" section and a "look-up" section, are analyzed. For each disector pair, the fractionator (*43*) is used to establish one sampling site that is the area of the electron micrograph in layer IV of the visual cortex. Between 6 and 15 serial electron micrographs per tissue block were used for stereological analysis. DCVs were characterized by the presence of an electron-dense core and at least 50% of circumference surrounded by an intact identifiable double-membrane (*44*); clear-core vesicles were not quantified. The sections were analyzed for DCVs present in the reference section but not the look-up section. These DCVs were counted. DCVs present on both the reference section and look-up section were not counted. The formulas $DCV_v = Q/V_{dis}$ and $V_{dis} = A_{frame}TN$ were used to obtain DCV density, where DCV_v is DCV density, Q is the number of DCVs present in the reference section but not the look-up section, V_{dis} is the disector volume of the tissue through which the DCVs are counted, A_{frame} is the area of the superimposed counting frame, T is section thickness, and N is the number of sections through which the counting is done.

EM Analysis/Statistics

The SPSS (SPSS Inc., Chicago, IL) statistical package (version 16.0) was used to conduct statistical analyses. Independent Student's *t*-tests were used to determine statistical significance. For DCV quantification, a two-way ANOVA was conducted to determine statistical significance for effects of age (P15, P25) and genotype (WT, *Fmr1* KO) on 415 micrographs from 36 animals. For these analyses, $p < 0.05$ was considered statistically significant.

Electrochemistry

Chromaffin cells were prepared as previously described (*45*, *46*). Plates were maintained in a humidified, 5% CO_2 atmosphere at 37 °C for at least 24 h prior to experimentation. Brain slices were prepared containing the CP (*31*), SNr (*30*), and BNST (*32*). Slices were superfused in artificial cerebrospinal fluid at 37 °C for 35−40 min prior to recording. Measurements were made with carbon-fiber microelectrodes prepared using T650 carbon fibers (*47*). At chromaffin cells, recordings were made by amperometry with disk electrodes (*46*). Measurements of DA, NE, and 5-HT release in brain slices were made using fast-scan cyclic voltammetry at cylindrical electrodes as previously described (*30*).

Exocytosis at chromaffin cells was triggered by 0.5 s pressure ejection of 60 mM K^+ buffer from a pipet located 30 μm from the cell. Ten stimulations, separated by 30 s, were applied to each cell. In brain slices, release was electrically evoked (*31*). Amperometric spikes were analyzed with MiniAnalysis (Synaptosoft, Decatur, GA). Individual amperometric spike characteristics determined were the spike frequency, quantal size (Q), $t_{1/2}$, and amplitude (*48*). In the slice experiments, the maximal neurotransmitter concentrations measured following stimulation are reported.

Supporting Information Available

A list of the most prominent secreted peptides identified from WT synaptoneurosomes, vesicular release events at chromaffin cells from WT and *Fmr1* KO mice, and representative EM images from visual cortex of WT and *Fmr1* KO mice, together with quantification data. This material is available free of charge via the Internet at http://pubs.acs.org.

Author Information

Corresponding Author

* Jonathan V. Sweedler, Eiszner Family Professor of Chemistry, Department of Chemistry, University of Illinois, 600 S. Mathews, Urbana, IL 61801, e-mail jsweedle@illinois.edu. William T. Greenough, Swanlund Professor of Psychology and Psychiatry, Beckman Institute, University of Illinois, 405 N. Mathews, Urbana, IL 61801, e-mail wgreenou@illinois.edu.

Author Contributions

S.P.A., S.H.K, J.V.S., B.M.K., K.T.T., R.M.W., W.T.G., and I.J.W. designed the research, S.P.A., A.E.L., S.H.K., S. R., B.M.K., K.T.T., and N.G.H. performed the research, S. P.A, B.M.K., K.T.T., and A.E.L. analyzed the data, and S.P. A., A.E.L., S.H.K., I.J.W., J.V.S., R.M.W., and W.T.G. wrote the paper.

Funding Sources

The projected described was supported by the National Institute on Drug Abuse (NIDA) under Award Nos. P30DA018310 and DA017940, the National Institute of Neurological Disorders and Stroke (NINDS) under Award Nos. NS031609 and NS038879, and the National Institute of Mental Health (NIMH) under Award No. MH035321. The content is solely the responsibility of the authors and does not necessarily represent the official views of the NIDA, NINDS, NIMH, or the National Institutes of Health.

Acknowledgment

We thank Dr. G. Govindaiah for technical assistance with brain slice techniques. We also thank Dr. Deepa Venkitaramani and Shawn Kohler for assistance with statistical analysis of DCV quantification. We gratefully acknowledge Stephanie Baker for help with manuscript preparation.

References

1. Turner, G., Webb, T., Wake, S., and Robinson, H. (1996) Prevalence of fragile X syndrome. *Am. J. Med. Genet. 64*, 196–197.

2. Fu, Y. H., Kuhl, D. P., Pizzuti, A., Pieretti, M., Sutcliffe, J. S., Richards, S., Verkerk, A. J., Holden, J. J., Fenwick, R. G.Jr., and Warren, S. T.; et al. (1991) Variation of the CGG repeat at the fragile X site results in genetic instability: Resolution of the Sherman paradox. *Cell 67*, 1047–1058.

3. Oberle, I., Rousseau, F., Heitz, D., Kretz, C., Devys, D., Hanauer, A., Boue, J., Bertheas, M. F., and Mandel, J. L. (1991) Instability of a 550-base pair DNA segment and abnormal methylation in fragile X syndrome. *Science 252*, 1097–1102.

4. Dictenberg, J. B., Swanger, S. A., Antar, L. N., Singer, R. H., and Bassell, G. J. (2008) A direct role for FMRP in

© 2010 American Chemical Society

activity-dependent dendritic mRNA transport links filopodial-spine morphogenesis to fragile X syndrome. *Dev. Cell 14*, 926–939.

5. Miyashiro, K. Y., Beckel-Mitchener, A., Purk, T. P., Becker, K. G., Barret, T., Liu, L., Carbonetto, S., Weiler, I. J., Greenough, W. T., and Eberwine, J. (2003) RNA cargoes associating with FMRP reveal deficits in cellular functioning in Fmr1 null mice. *Neuron 37*, 417–431.

6. Brown, V., Jin, P., Ceman, S., Darnell, J. C., O'Donnell, W. T., Tenenbaum, S. A., Jin, X., Feng, Y., Wilkinson, K. D., Keene, J. D., Darnell, R. B., and Warren, S. T. (2001) Microarray identification of FMRP-associated brain mRNAs and altered mRNA translational profiles in fragile X syndrome. *Cell 107*, 477–487.

7. Dolen, G., Osterweil, E., Rao, B. S., Smith, G. B., Auerbach, B. D., Chattarji, S., and Bear, M. F. (2007) Correction of fragile X syndrome in mice. *Neuron 56*, 955–962.

8. Hayashi, M. L., Rao, B. S., Seo, J. S., Choi, H. S., Dolan, B. M., Choi, S. Y., Chattarji, S., and Tonegawa, S. (2007) Inhibition of p21-activated kinase rescues symptoms of fragile X syndrome in mice. *Proc. Natl. Acad. Sci. U.S.A. 104*, 11489–11494.

9. Godfraind, J.-M., Reyniers, E., Boulle, K. D., D'Hooge, R., DeDeyn, P. P., Bakker, C. E., Oostra, B. A., Kooy, R. F., and Willems, P. J. (1996) Long-term potentiation in the hippocampus of fragile X knockout mice. *Am. J. Med. Genet. 64*, 246–251.

10. Huber, K. M., Gallagher, S. M., Warren, S. T., and Bear, M. F. (2002) Altered synaptic plasticity in a mouse model of fragile X mental retardation. *Proc. Natl. Acad. Sci. U.S.A. 99*, 7746–7750.

11. Consortium, T. D.-B. F. X., Bakker, C. E., Verheij, C., Willemsen, R., van der Helm, R., Oerlemans, F., Vermey, M., Bygrave, A., Hoogeveen, A., Oostra, B. A., Reyniers, E., De Boule, K., D'Hooge, R., Cras, P., van Velzen, D., Nagels, G., Martin, J.-J., De Deyn, P. P., Darby, J. K., and Willems, P. J. (1994) Fmr1 knockout mice: A model to study fragile X mental retardation. *Cell 78*, 23–33.

12. Irwin, S. A., Idupulapati, M., Gilbert, M. E., Harris, J. B., Chakravarti, A. B., Rogers, E. J., Crisostomo, R. A., Larsen, B. P., Mehta, A., Alcantara, C. J., Patel, B., Swain, R. A., Weiler, I. J., Oostra, B. A., and Greenough, W. T. (2002) Dendritic spine and dendritic field characteristics of layer V pyramidal neurons in the visual cortex of fragile-X knockout mice. *Am. J. Med. Genet. 111*, 140–146.

13. Hanson, J. E., and Madison, D. V. (2007) Presynaptic FMR1 genotype influences the degree of synaptic connectivity in a mosaic mouse model of fragile X syndrome. *J. Neurosci. 27*, 4014–4018.

14. Lauterborn, J. C., Rex, C. S., Kramar, E., Chen, L. Y., Pandyarajan, V., Lynch, G., and Gall, C. M. (2007) Brain-derived neurotrophic factor rescues synaptic plasticity in a mouse model of fragile X syndrome. *J. Neurosci. 27*, 10685–10694.

15. Geppert, M., Goda, Y., Stevens, C. F., and Sudhof, T. C. (1997) The small GTP-binding protein Rab3A regulates a late step in synaptic vesicle fusion. *Nature 387*, 810–814.

16. Leenders, A. G. M., da Silva, F. H. L., Ghijsen, W. E. J. M., and Verhage, M. (2001) Rab3A is involved in transport of synaptic vesicles to the active zone in mouse brain nerve terminals. *Mol. Biol. Cell 12*, 3095–3102.

17. Liao, L., Park, S. K., Xu, T., Vanderklish, P., and Yates, J. R.3rd (2008) Quantitative proteomic analysis of primary neurons reveals diverse changes in synaptic protein content in Fmr1 knockout mice. *Proc. Natl. Acad. Sci. U.S.A. 105*, 15281–15286.

18. Castillo, P. E., Janz, R., Sudhof, T. C., Tzounopoulos, T., Malenka, R. C., and Nicoll, R. A. (1997) Rab3A is essential for mossy fibre long-term potentiation in the hippocampus. *Nature 388*, 590–593.

19. Sakane, A., Manabe, S., Ishizaki, H., Tanaka-Okamoto, M., Kiyokage, E., Toida, K., Yoshida, T., Miyoshi, J., Kamiya, H., Takai, Y., and Sasaki, T. (2006) Rab3 GTPase-activating protein regulates synaptic transmission and plasticity through the inactivation of Rab3. *Proc. Natl. Acad. Sci. U.S.A. 103*, 10029–10034.

20. van Weering, J. R. T., Toonen, R. F., and Verhage, M. (2007) The role of Rab3a in secretory vesicle docking requires association/dissociation of guanidine phosphates and Munc18-1. *PLoS ONE 2*, No. e616.

21. Wilson, B. M., and Cox, C. L. (2007) Absence of metabotropic glutamate receptor-mediated plasticity in the neocortex of fragile X mice. *Proc. Natl. Acad. Sci. U.S.A. 104*, 2454–2459.

22. Ghijsen, W. E., Leenders, A. G., and Lopes da Silva, F. H. (2003) Regulation of vesicle traffic and neurotransmitter release in isolated nerve terminals. *Neurochem. Res. 28*, 1443–1452.

23. Rubakhin, S. S., Churchill, J. D., Greenough, W. T., and Sweedler, J. V. (2006) Profiling signaling peptides in single mammalian cells using mass spectrometry. *Anal. Chem. 78*, 7267–7272.

24. Rubakhin, S. S., and Sweedler, J. V. (2007) Characterizing peptides in individual mammalian cells using mass spectrometry. *Nat. Protoc. 2*, 1987–1997.

25. Hatcher, N. G., Atkins, N., Jr., Annangudi, S. P., Forbes, A. J., Kelleher, N. L., Gillette, M. U., and Sweedler, J. V. (2008) Mass spectrometry-based discovery of circadian peptides. *Proc. Natl. Acad. Sci. U.S.A. 105*, 12527–12532.

26. Hatcher, N. G., Richmond, T. A., Rubakhin, S. S., and Sweedler, J. V. (2005) Monitoring activity-dependent peptide release from the CNS using single-bead solid-phase extraction and MALDI TOF MS detection. *Anal. Chem. 77*, 1580–1587.

27. Hatcher, N. G., and Sweedler, J. V. (2008) *Aplysia* bag cells function as a distributed neurosecretory network. *J. Neurophysiol. 99*, 333–343.

28. Jing, J., Vilim, F. S., Horn, C. C., Alexeeva, V., Hatcher, N. G., Sasaki, K., Yashina, I., Zhurov, Y., Kupfermann, I., Sweedler, J. V., and Weiss, K. R. (2007) From hunger to satiety: Reconfiguration of a feeding network by *Aplysia* neuropeptide Y. *J. Neurosci. 27*, 3490–3502.

29. Zakharenko, S. S., Patterson, S. L., Dragatsis, I., Zeitlin, S. O., Siegelbaum, S. A., Kandel, E. R., and Morozov, A.

© 2010 American Chemical Society

DOI: 10.1021/cn900036x | *ACS Chem. Neurosci.* (2010), *1*, 306–314

(2003) Presynaptic BDNF required for a presynaptic but not postsynaptic component of LTP at hippocampal CA1-CA3 synapses. *Neuron 39*, 975–990.

30. Bunin, M. A., Prioleau, C., Mailman, R. B., and Wightman, R. M. (1998) Release and uptake rates of 5-hydroxytryptamine in the dorsal raphe and substantia nigra reticulata of the rat brain. *J. Neurochem. 70*, 1077–1087.

31. Johnson, M. A., Rajan, V., Miller, C. E., and Wightman, R. M. (2006) Dopamine release is severely compromised in the R6/2 mouse model of Huntington's disease. *J. Neurochem. 97*, 737–746.

32. Miles, P. R., Mundorf, M. L., and Wightman, R. M. (2002) Release and uptake of catecholamines in the bed nucleus of the stria terminalis measured in the mouse brain slice. *Synapse 44*, 188–197.

33. Shakiryanova, D., Tully, A., Hewes, R. S., Deitcher, D. L., and Levitan, E. S. (2005) Activity-dependent liberation of synaptic neuropeptide vesicles. *Nat. Neurosci. 8*, 173–178.

34. Torrealba, F., and Carrasco, M. A. (2004) A review on electron microscopy and neurotransmitter systems. *Brain Res. Rev. 47*, 5–17.

35. Li, L., and Sweedler, J. V. (2008) Peptides in our brain: Mass spectrometric-based measurement approaches and challenges. *Annu. Rev. Anal. Chem. 1*, 451–483.

36. Zhao, M.-G., Toyoda, H., Ko, S. W., Ding, H.-K., Wu, L.-J., and Zhuo, M. (2005) Deficits in trace fear memory and long-term potentiation in a mouse model for fragile X syndrome. *J. Neurosci. 25*, 7385–7392.

37. Vaughn, J. E. (1989) Fine structure of synaptogenesis in the vertebrate central nervous system. *Synapse 3*, 255–285.

38. Ziv, N. E., and Garner, C. C. (2004) Cellular and molecular mechanisms of presynaptic assembly. *Nat. Rev. Neurosci. 5*, 385–399.

39. Fischer, M., Kaech, S., Knutti, D., and Matus, A. (1998) Rapid actin-based plasticity in dendritic spines. *Neuron 20*, 847–854.

40. Bora, A., Annangudi, S. P., Millet, L. J., Rubakhin, S. S., Forbes, A. J., Kelleher, N. L., Gillette, M. U., and Sweedler, J. V. (2008) Neuropeptidomics of the supraoptic rat nucleus. *J. Proteome Res. 7*, 4992–5003.

41. Greenough, W. T., Klintsova, A. Y., Irwin, S. A., Galvez, R., Bates, K. E., and Weiler, I. J. (2001) Synaptic regulation of protein synthesis and the fragile X protein. *Proc. Natl. Acad. Sci. U.S.A. 98*, 7101–7106.

42. Sterio, D. C. (1984) The unbiased estimation of number and sizes of arbitrary particles using the disector. *J. Microsc. 134*, 127–136.

43. Gundersen, H. J., Bagger, P., Bendtsen, T. F., Evans, S. M., Korbo, L., Marcussen, N., Moller, A., Nielsen, K., Nyengaard, J. R., and Pakkenberg, B. (1988) The new stereological tools: Disector, fractionator, nucleator and point sampled intercepts and their use in pathological research and diagnosis. *APMIS 96*, 857–881.

44. Umbach, J. A., Zhao, Y., and Gundersen, C. B. (2005) Lithium enhances secretion from large dense-core vesicles in nerve growth factor-differentiated PC12 cells. *J. Neurochem. 94*, 1306–1314.

45. Kolski-Andreaco, A., Cai, H., Currle, D. S., Chandy, K. G., and Chow, R. H. (2007) Mouse adrenal chromaffin cell isolation. *J. Vis. Exp.*129.

46. Villanueva, M., Thornley, K., Augustine, G. J., and Wightman, R. M. (2006) Synapsin II negatively regulates catecholamine release. *Brain Cell Biol. 35*, 125–136.

47. Cahill, P. S., Walker, Q. D., Finnegan, J. M., Mickelson, G. E., Travis, E. R., and Wightman, R. M. (1996) Microelectrodes for the measurement of catecholamines in biological systems. *Anal. Chem. 68*, 3180–3186.

48. Colliver, T. L., Hess, E. J., Pothos, E. N., Sulzer, D., and Ewing, A. G. (2000) Quantitative and statistical analysis of the shape of amperometric spikes recorded from two populations of cells. *J. Neurochem. 74*, 1086–1097.

© 2010 American Chemical Society

DOI: 10.1021/cn900036x | *ACS Chem. Neurosci.* (2010), *1*, 306–314